# Supplementary Information

## Volcano-shaped SPM probe for combined force-electrogram recordings from excitable cells

B.X.E. Desbiolles[1], M.T.M Hannebelle[2], E. de Coulon[3], A. Bertsch[1], S. Rohr[3], G. E. Fantner[2], and P. Renaud[1]

## Table of content



[1] Laboratory of Microsystems LMIS4, Ecole Polytechnique Fédérale de Lausanne, Lausanne, Switzerland.

[2] Laboratory of Bio- and Nano- Instrumentation, Ecole Polytechnique Fédérale de Lausanne, Lausanne, Switzerland.

[3] Group Rohr, Department of Physiology, University of Bern, Bern, Switzerland

Correspondence: Benoit Xavier Emmanuel Desbiolles (benoit.desbiolles@epfl.ch)

# 1 Mechanical and electrical interfacing

## 1.1 Custom cantilever holder

A custom interface was necessary to connect the nanovolcano probe to both the AFM and the electronic measurement system. A custom-made shielded PCB connected to a 800 µm-diameter U. FL coaxial cable was screwed to a custom-made AFM cantilever holder as illustrated in Figure S1-A. Figure S1-B shows the nanovolcano probe glued to the PCB and wire-bonded to the gold coated pad of the PCB. The PCB directly connects the gold coated pad to the inner wire of the coaxial output, therefore guaranteeing an standard electrical connection to the nanovolcano. A glob top was used to electrically insulate the chip-PCB interface when the system is immersed in liquid (cf. Figure S1-C). Overall, this interface prevents any electrical shortcut when working in a liquid environment, and shields the recorded electrical signals from external electromagnetic noises, therefore allowing for low-noise recordings.

The cantilever holder keeps the nanovolcano probe tilted at an angle of 11° with respect to the horizontal, as required for the optical deflection measurement with AFM.

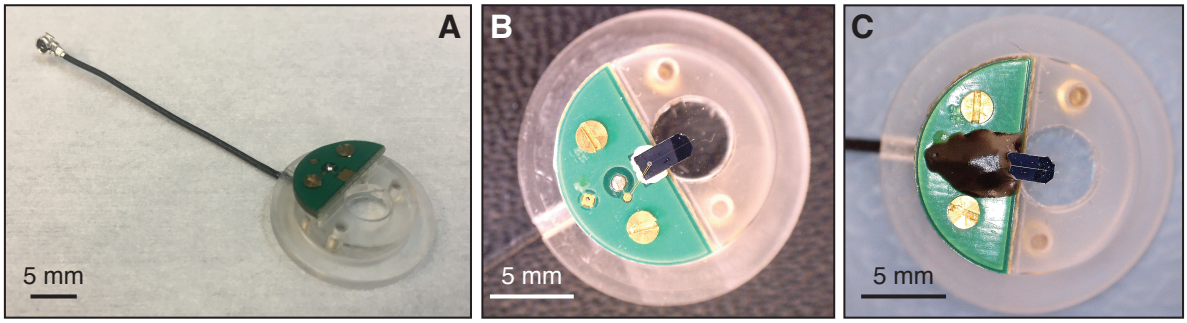


**Figure S1:** *Mechanical and electrical interfacing of the nanovolcano probe.* A) Picture of the custom-made AFM holder without the nanovolcano probe assembled. B) Top-view image of the nanovolcano probe mechanically assembled and wire-bonded to the custom-made holder. C) Top-view image of the interface with the glob top used to insulate the chip-PCB electrical contact.

## 1.2 Setup for simultaneous optical imaging, force, and electrical recordings

A custom setup was necessary to obtain simultaneously optical images as well as mechanical forces and electrical recordings (Figure S2-A). The cells were seeded to 6 cm in diameter petri dish, which was mounted in a custom sample holder. The cells were then covered with liquid medium (Figure S2-A). The sample holder rests on a large aluminum structure placed on a noise cancelling table (not represented in the figure) to ensure minimal mechanical noise. The

nanovolcano probe was placed on top of the sample using the custom cantilever holder described above (Figure S1), connected to a commercial tip-scanning AFM head (Figure S2). The cantilever deflection is measured using an optical laser readout. The force applied by the cell to the cantilever is calculated based the cantilever deflection signal, knowing the cantilever stiffness and deflection sensitivity. The nanovolcano cantilever electrode is connected through a coaxial cable to a microelectrode amplifier and a digital acquisition system to record the electrical signal. An inverted microscope was placed under the sample holder to allow for simultaneous optical imaging.

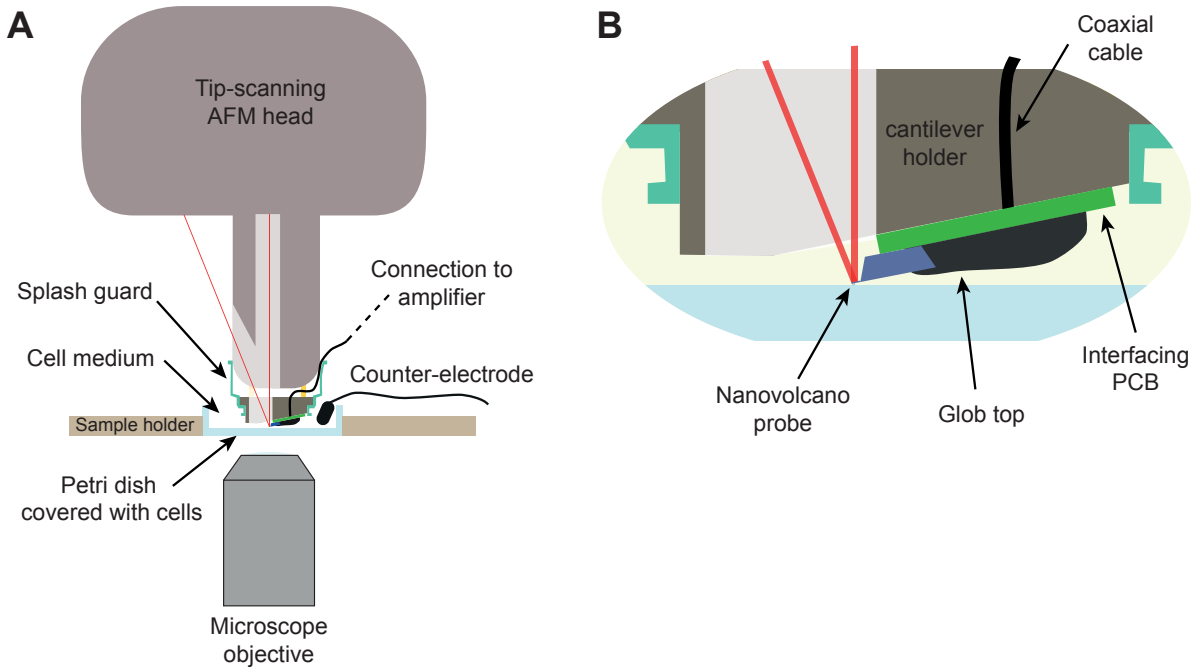


**Figure S2***: Description of the custom AFM-optical system*. A) Schematic drawing showing a cross-section view of the custom-made AFM-optical system. B) Expanded cross-section view of the custom-made cantilever holder mounted on the AFM head.

# 2 Electrochemical characterization

## 2.1 Electrode-electrolyte interface

Figure S3-A shows the electrical equivalent model of the electrode-electrolyte interface. As previously described in the literature,[1] it is composed of a non-linear resistance, $R_{CT}$, that represents faradaic charge transfer secondary to redox reactions, in parallel with a constant phase element $Z_{CPE,DL}$ representing the double layer capacitance underlying the capacitive charge transfer. $R_{Spread}$ represents the resistance induced the confinement of the electric field lines near the microelectrode. The stray capacitance, $C_{stray}$, denotes the capacitive current leaks along the insulated tracks.

The electrode-electrolyte interface properties have been experimentally measured using electrochemical impedance spectroscopy (EIS) based on a 100 mV sinusoidal signal applied to the nanovolcano probe in presence of phosphate buffer saline (PBS) at room temperature. The EIS data are shown in Figure S3-B and show a typical electrode-electrolyte behavior.[2] Values for each element composing the electrical equivalent circuit have been extracted and are summarized in Table S1.

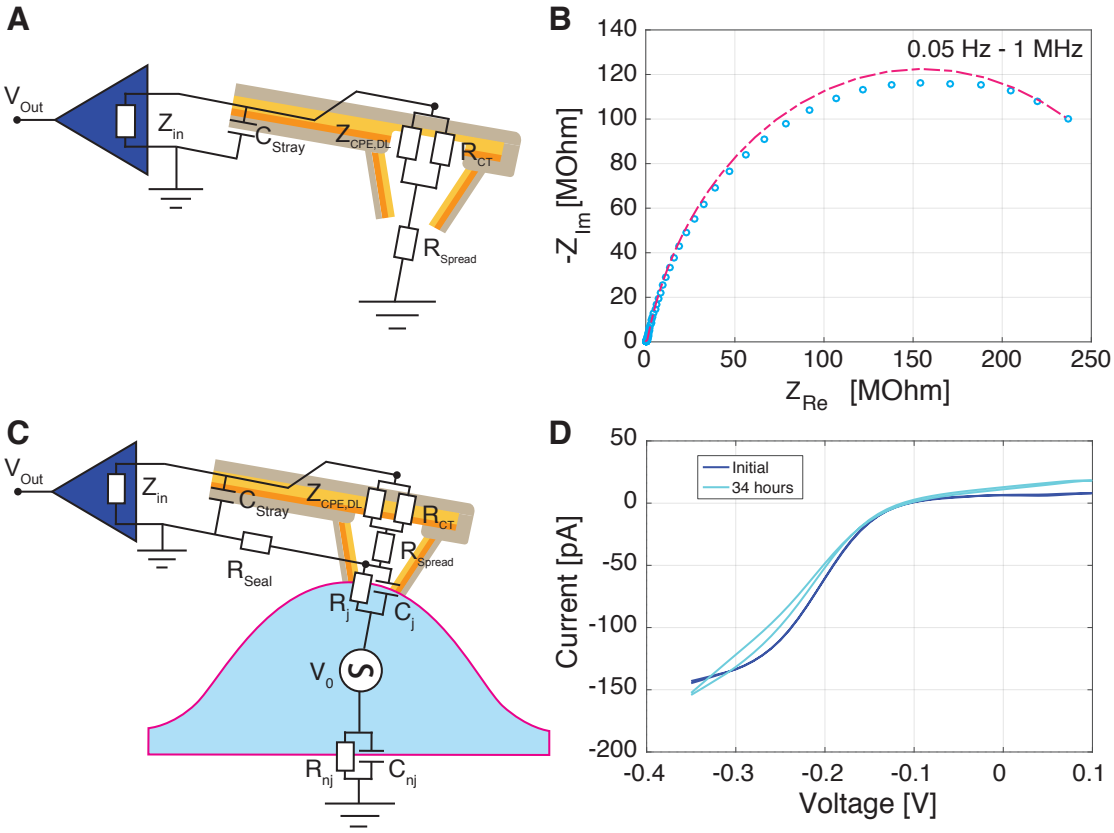


**Figure S3:** *Electrochemical characterization of the nanovolcano probe.* A) Equivalent electrical model of the electrode-electrolyte interface. B) Electrochemical impedance spectroscopy of a single nanovolcano probe in PBS. C) Equivalent electrical model of the cell-electrode interface. D) Cyclic voltammogram of the nanovolcano probe right after immersion in a solution of 5 mM hexaamine ruthenium chloride and 100 mM potassium nitrate in deionized water (dark blue) and after 34 hours of continuous chronoamperometry at a fixed potential of -0.35 V (light blue).

**Table S1:** Experimental values of every element composing the electrical equivalent circuit of the electrode-electrolyte interface

| Element | Value |
|---|---|
| $R_{CT}$ | 315 MΩ |
| $C_{DL}$, $n$ | 4.15 nF, 0.82 |
| $R_{Spread}$ | 74.4 kΩ |
| $C_{Stray}$ | 30 pF |

## 2.2 Cell-electrode interface

Figure S3-C represents the electrical equivalent circuit once the nanovolcano probe is engaged onto a cell. In this situation, the junctional membrane resistance $R_j$ and capacitance $C_j$ are added in parallel with the seal resistance $R_{seal}$, representing the leaks at the cell-electrode interface, at the tip of the nanovolcano probe. $V_0$ is the cell transmembrane potential whereas $R_{nj}$ and $C_{nj}$ respectively represent the non-junctional cell membrane resistance and capacitance.

During engaging, no variation of the resistance is observed at low frequency; therefore suggesting that the seal resistance $R_{Seal}$ is much lower compared to the charge transfer resistance $R_{CT}$. However, at higher frequency, the impedance of the electrode-electrolyte interface ($Z_{CPE,DL} \parallel R_{CT}$) becomes negligible as most of the current passes through the low double layer impedance. At this frequency, impedance measurements (as reported in Figure 2, main manuscript) directly represent the spreading resistance in serial with the other components of the cell-electrode interface ($R_{Seal} \parallel R_j \parallel C_j$). For this reason, the impedance and time constant seen by the nanovolcano probe increases when approaching the cell surface.

## 2.3 Long-term characterization

The long-term stability of the nanovolcano probe was characterized by Scuba Probe Technologies LLC. The nanovolcano probe was immersed into a solution of 5 mM hexaamine ruthenium chloride and 100 mM potassium nitrate in deionized water. As shown in Figure S3-D, a first cyclic voltammogram was acquired between -0.35 V to 0.1 V vs. Ag/AgCl at a scan rate of 50 mV/s using a 3 electrodes setup (dark blue curve). For the next 34 hours, the nanovolcano potential was hold at -0.35 V while similar cyclic voltammograms were registered every 20 minutes as control. The light blue cyclic voltammogram in Figure S3-D shows nearly no significant differences compared to the initial one, thereby demonstrating that the nanovolcano probe was functional for 34 hours.

# 3 Additional data

In this section, additional data recorded with the nanovolcano probe are presented to demonstrate the reliability of the method.

## 3.1 Force-controlled impedance measurements

Overall, force-controlled impedance measurements were performed on seven human embryonic kidney (HEK) cells and seven primary rat cardiomyocytes (CMCs) using two different nanovolcano probes. Experimental results are summarized in Table S2.

**Table S2:** Summary of the force-controlled impedance measurements performed on human embryonic kidney cells and primary rat cardiomyocytes.

| Cell ID | Cell type | Probe | Impedance Z [kΩ] | | | Time constant $\tau$ [µs] | | | Peak force [nN] | Ramp rate [Hz] |
|---|---|---|---|---|---|---|---|---|---|---|
| | | | Off cell | On cell | ΔZ [%] | Off cell | On cell | $\Delta\tau$ [%] | | |
| **1** | HEK | 1 | 458 | 502 | 109 | 30 | 40 | 133 | 15 | 0.25 |
| **2** | HEK | 2 | 361 | 485 | 131 | 25 | 35 | 140 | 400 | 0.1 |
| **3** | HEK | 2 | 358 | 640 | 178 | 25 | 45 | 180 | 22.1 | 0.1 |
| **4** | HEK | 2 | 400 | 850 | 212 | 25 | 40 | 160 | 60 | 0.1 |
| **5** | HEK | 2 | 426 | 594 | 139 | 25 | 30 | 120 | 12 | 1 |
| **6** | HEK | 2 | 440 | 820 | 186 | 25 | 35 | 140 | 115 | 1 |
| **7** | HEK | 2 | 441 | 718 | 163 | 25 | 35 | 140 | 19.5 | 0.1 |
| **8** | CMC | 2 | 493 | 993 | 201 | 35 | 65 | 186 | 470 | 2 |
| **9** | CMC | 2 | 458 | 601 | 131 | 30 | 45 | 150 | 36 | 3 |
| **10** | CMC | 2 | 467 | 496 | 106 | 30 | 35 | 117 | 15.5 | 3 |
| **11** | CMC | 2 | 498 | 941 | 195 | 35 | 56 | 160 | 772 | 2 |
| **12** | CMC | 2 | 507 | 561 | 111 | 35 | 40 | 114 | 46 | 3 |
| **13** | CMC | 2 | 494 | 560 | 113 | 30 | 35 | 117 | 12.5 | 3 |
| **14** | CMC | 2 | 432 | 625 | 145 | 30 | 40 | 133 | 43 | 3 |

## 3.2 Contraction displacement measurements

Contraction characteristics recorded from five different primary rat cardiomyocytes are summarized in Table S3. Parameters include the contraction amplitude, duration at 50% of the amplitude, contraction number, as well as the overall recording duration for each cell tested.

**Table S3:** Summary of the primary rat cardiomyocyte contraction characteristics recorded from different cells with a single nanovolcano probe (mean ± SD).

| Cell ID | Contraction amplitude [nm] | Contraction duration [s] | Number of contractions | Recording duration [s] |
|---|---|---|---|---|
| **1** | 382 ± 95 | 415 ± 117 | 11 | 50 |
| **2** | 262 ± 88 | 436 ± 26 | 12 | 25 |
| **3** | 207 ± 28 | 545 ± 78 | 6 | 7 |
| **4** | 26 ± 3 | 231 ± 124 | 3 | 3 |
| **5** | 121 ± 44 | 297 ± 18.1 | 19 | 50 |

### 3.3 Electrogram measurements

Overall, two electrograms were successively recorded from two different cells using a single nanovolcano probe, therefore demonstrating the capability of successive recordings at different location with a single probe. The signals of the first recording are presented in main manuscript Figure 4, those of the second recording are shown in Figure S4. Electrograms displayed downstroke amplitudes of 64 ± 17 µV (N = 42) for an overall recording duration of 25 s.

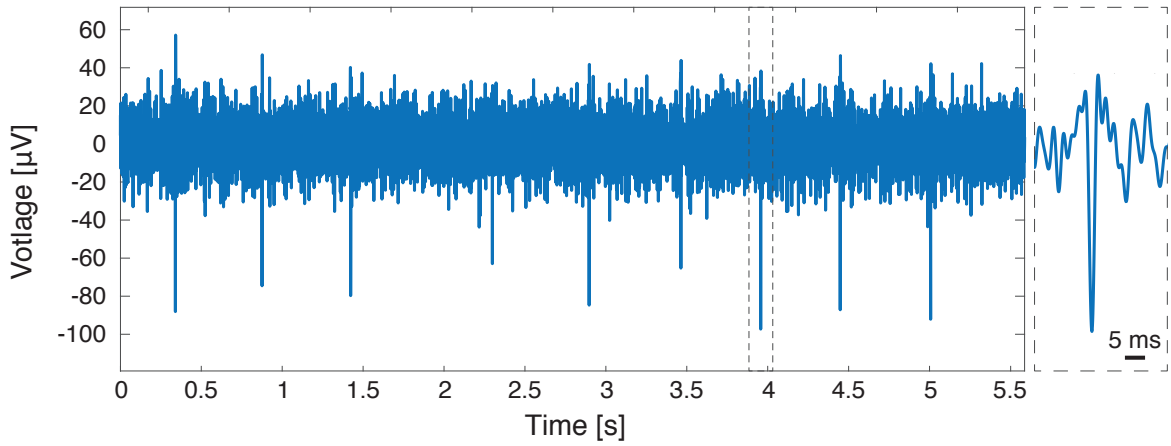


**Figure S4:** Recording of a cardiomyocyte electrogram using the nanovolcano probe. The insert presents an expanded view of the region of the electrogram framed with dashed lines.

## 4 References


1. B. X. E. Desbiolles, E. De Coulon, A. Bertsch, S. Rohr and P. Renaud, Intracellular Recording of Cardiomyocyte Action Potentials with Nanopatterned Volcano-Shaped Microelectrode Arrays, *Nano Letters*, 19, 6173–6181, **2019**.

2. W. Franks, I. Schenker, P. Schmutz and A. Hierlemann, Impedance characterization and modeling of electrodes for biomedical applications, *IEEE Transactions on Biomedical Engineering*, 52, 1295–1302, **2005**.